1
2
3
4
5
6
7
8
9

A Ballistic Pollen Dispersal Strategy Based on Stylar Oscillation

of *Hypochaeris radicata* (Asteraceae)

Shuto Ito*, Hamed Rajabi, Stanislav N Gorb

Department of Functional Morphology and Biomechanics, University of Kiel, Am Botanischen Garten 9, D-24118 Kiel, Germany

* corresponding author

19   Abstract

20

21   Asteraceae, one of the largest flowering plant families, is adapted to a vast range of

22   ecological niches. Their adaptability is partially based on their strong ability to reproduce.

23   The initial, yet challenging, step for the reproduction of animal-pollinated plants is to

24   transport pollen to flower-visiting pollinators. We adopted *Hypochaeris radicata* as a model

25   species to investigate the functional morphology of the typical floral feature of Asteraceae, a

26   pollen-bearing style. Using quantitative experiments and numerical simulations, here we

27   show that the pollen-bearing style can serve as a ballistic lever for catapulting pollen grains

28   to pollinators. This can potentially be a pollen dispersal strategy to propel pollen to safe

29   sites of pollinators' bodies, which are beyond the physical reach of the styles. Our results

30   suggest that the specific morphology of the floret and the pollen adhesion avoid pollen

31   waste by catapulting pollen within a specific range equal to the size of a flowerhead. The

32   insights into the functional floral oscillation may shed light on the superficially

33   unremarkable, but ubiquitous functional floral design of Asteraceae.

34

35

1. Introduction

Animal-mediated pollination is a complex interaction between plants and pollinators with conflicting interests. Plants strive for efficient and reliable pollen dispersal, whereas pollinators seek floral rewards that can be harvested as efficiently as possible[1,2]. Plants employ various strategies to attract pollinators and ensure efficient pollen dispersal. One common approach is to offer floral rewards, such as nectar and pollen, to entice pollinators and facilitate direct physical contact between the exposed pollen grains and the floral visitors. To enhance this process, many plants have diversified their morphologies, such as corolla tube[3,4], staminal lever[5], trapping device[6], or even sexual deception through the use of petals[7]. In contrast, there are other dynamic pollination strategies without involving direct contact between the presented pollen and pollinators, such as explosive pollen release[8–10] and buzz pollination[11–16]. In this paper, we focus on a ubiquitous floral feature of Asteraceae and aimed to shed light on previously unexplored dynamic pollen dispersal mechanics in the plant family.

The Asteraceae family, with over 23,000 species making up roughly 10% of all flowering plants, is widely distributed on every continent except Antarctica[17]. These plants are characterized by their tightly packed inflorescences, or flower heads, comprised of numerous individual flowers, known as florets (Fig. 1). Pollination in the Asteraceae family is initiated by the release of pollen grains into anther tube, which pushes or brushes the pollen out and exposes it at the stylar surface[18,19]. The flowers of Asteraceae are visited by a diverse range of pollinators, making them considered generalists[20]. However, some visitors utilize their elongated mouthparts to obtain nectar without frequently contacting the exposed pollen grains (Fig. 2f-h), potentially leading to insufficient pollen transfer for successful pollination. Corbiculate bees have refined pollen-collection methods using adhesive saliva and a pollen-collecting apparatus[21–24], but without strategies to prevent excess pollen collection, the costs of attracting such pollinators can outweigh the benefits. While dynamic pollination strategies, such as explosive pollen release and buzz pollination, have been documented in other plant families, they have not been documented in Asteraceae. In this study, we examine the feasibility of transferring pollen to pollinators without direct physical contact through the oscillation of a pollen-bearing style. Our objective is to uncover a previously undocumented mode of pollen dispersal in a typical flower of the Asteraceae family through quantitative experiments and numerical simulations.

2. Material and methods

2.1. Plant Species

Hypochaeris radicata (Asteraceae) was previously adopted as a model species to investigate pollen adhesion[25,26]. In this paper, this species was used, to study the motion of pollen-bearing styles and the resulting pollen dispersal. *H. radicata* is a perennial plant, native to Europe, and currently is a cosmopolitan invasive species occurring in a wide range of temperate zones, including America, Japan, and Australia[27]. *H. radicata* is known to be self-incompatible. This means that the successful transport of pollen grains to different individual plants of the same species is of necessity to enable its healthy reproduction[28]. Flowering stems of *H. radicata* were collected in Kiel, Germany, for experimentation. They were placed in water until the youngest florets exposed fresh pollen.

2.2. Field observations

To observe the pollen-collecting behaviors of pollinators on flowerheads of *H. radicata,* we filmed videos in slow motion (120 fps) by using an iPhone 7 (Apple Inc., California, USA) together with a 30x magnifying glass (Fig. 2c-e).

2.3. Mechanical characterization of florets

We collected the newly opened florets from the flower heads and analyzed the morphology of the florets under a light microscope (Leica Microsystem, Wetzlar, Germany) (Fig. 1). In order to characterize the mechanical properties of the florets, we measured the spring constant of the following segments: (1) styles, (2) anther tubes, and (3) filaments. Fig. 3a illustrates the experimental setup used for this purpose. Each freshly opened floret was first horizontally fixed between two wooden blocks. We fixed the floret specimens at different positions to measure the spring constant of their different segments (right-hand sketch in Fig. 3b): (1) The entire anther tube was fixed to test the style (fixation at f_1), (2) the basal part of the anther tube including the filaments was fixed to test the anther tube (fixation at f_2),

and (3) the basal part of the petal was fixed to test the filaments (fixation at f_3). Floret specimens were deflected using a thin metallic part mounted onto a force transducer (10g capacity; World Precision Instruments Inc., Sarasota, FL, USA). The deflections were always applied at 1 mm distal to the fixation positions at a controlled displacement speed of 0.01 mm/sec. The required force to deflect the specimens was continuously recorded using AcqKnowledge 3.7.0 software (Biopac Systems Ltd, Goleta, CA, USA). To measure the spring constant of the floret specimens, we always used the data from the initial part of obtained force-displacement curves (limited to a displacement equal to 50 μm). In total, we tested 34 florets including 9 tests on styles, 10 on anther tubes, and 15 on filaments. Each floret was subjected to a single test and was not used again.

2.3. Stylar oscillation experiments

Black circular polyethylene plates with a hole at the center were prepared for visualizing the distribution of pollen grains catapulted by stylar oscillations. Each newly opened floret was vertically fixed through the hole of the plate onto the vise to stand upright (Fig. 4). To examine whether the pollen dispersal caused by the stylar oscillation depends on the magnitude of an initial deflection, an insect pin attached to a micro-manipulator (World Precision Instruments, FL, USA) was brought in contact with one of the two following segments of the standing floret: (1) the style and (2) anther tube (Fig. 4). The contact with the anther tube resulted in a large deflection of the floret, while the contact with the style caused a smaller deflection. The insect pin was kept moving horizontally until the deflected floret was released (Figs. 2i-k, 4). After the release, the floret started to oscillate and this led to the release of clumps of pollen grains, here called 'dispersal units' (DU), from the style (Fig. 2j-k). The oscillations were filmed by a high-speed camera (Olympus, Tokyo, Japan) at 5000 fps and tracked using open-source tracking software (Tracker by Douglas Brown)[29]. In total, we analyzed the stylar oscillations of 55 specimens, among which 24 specimens were used to analyze the distribution and the number of pollen grains catapulted by the oscillations.

Assuming linearity of the oscillatory system, the damping ratio, ζ, of a floret was obtained based on the logarithmic decrement, δ:

$$\delta = \frac{1}{i} ln \frac{a_1}{a_i}, \tag{1}$$

Where a_1 and a_i are the amplitudes of the first peak and the peak, which is $i-1$ periods away, respectively. By using eq.1, we obtained the damping ratio, ζ:

137
$$\zeta = \frac{1}{\sqrt{1 + (\frac{2\pi}{\delta})^2}}. \qquad (2)$$

138   The dispersal units that landed on the plate were photographed under a microscope

139   (Keyence, Osaka, Japan). The images were analyzed by a custom script in MATLAB

140   (Mathworks, Natick, USA) to obtain dispersal distances. To count the number of dispersed

141   pollen grains, the grains on the plate were collected, placed in a droplet of mineral oil on a

142   glass slide, and sandwiched with a glass coverslip to spread out as a single layer. They were

143   then photographed in a microscope (Leica Microsystem, Wetzlar, Germany). Using the

144   images, the grains were counted by a custom script in MATLAB.

145

146   2.4. Numerical simulation of trajectories of dispersal units

147

148   Due to the technical difficulties of tracking single dispersal units based on the high-speed

149   videos, we computed trajectories of dispersal units and their dispersal distances. During the

150   stylar acceleration, dispersal units on the style experience inertia. They could leave the style

151   if the inertial force exceeds the attachment force of the dispersal units on the stylar surface.

152   The inertial force, F_i, required to detach a dispersal unit from the style can be obtained from:

153
$$F_i = mn a_c = c F_a , \qquad (3)$$

154   where a_c is the critical acceleration, F_a is the adhesion force of the pollen on the style, c is the

155   number of contact points between a dispersal unit and the style, m is the mass of single

156   pollen grains, and n is the number of pollen grains forming a single dispersal unit.

157   The adhesion of pollen grains has already been measured for *H. radicata* on the stylar

158   surface: median adhesion force, F_a, was 98 nN (N = 50) [26]. The mass of individual pollen

159   grains, m, is 15.0 ± 0.4 ng[25]. The number of pollen grains forming a single dispersal unit, n,

160   was determined by dividing the number of dispersed grains by the number of dispersal

161   units (N = 24, n = 12.9 ± 5.3). The number of contact points, c, was set as 2 to restrict major

162   pollen dispersal to the first cycle of oscillations, as observed in experiments. Using these

163   data, the critical acceleration that can detach a dispersal unit from the style was calculated,

164   and it was shown as a boxplot in Fig. 5c. In the numerical simulation, we used the median

165   value of the critical acceleration ($a_c = 1005 \text{ ms}^{-2}$).

166   We measured the stylar velocity, *v*, and acceleration, *a*, at different time frames using

167   the recorded high-speed videos (N = 55) (Fig. 7a, red asterisks). When the stylar acceleration

168   was greater than the critical acceleration, the trajectory of the dispersal unit was simulated

169   (Fig. 7a, solid curves). The initial position and velocity of each dispersal unit were set to be

equal to those of the styles. The initial position of a dispersal unit (x, y) is referred to here as the detachment point of that unit (Fig. 7b).

Here, we assumed the dispersal units to consist of 13 pollen grains ($n = 13$) based on the measurements, mentioned earlier. The diameter of the dispersal units can be calculated by[30]:

$$R = 3r, \tag{4}$$

where the radius of a single pollen grain, r, is equal to 15 μm[25].

Reynolds number at a given time, R_e, is given as:

$$R_e = \frac{2|v|R\rho}{\varphi}, \tag{5}$$

where v is the velocity of a dispersal unit at a given time, ρ is the density of air (1.204 kg/m³), and φ is the dynamic viscosity of air at 20℃ (1.825×10^{-7} kgm⁻¹s⁻¹). Considering the low range of Reynolds number ($0.3 < Re < 8.5$), the drag coefficient C_d is not constant, instead is calculated by the following empirical relationship[31]:

$$C_D = \frac{24}{R_e}\left(1 + \frac{3R_e}{16}\right). \tag{6}$$

Once C_d is obtained, the drag force, $D(t)$, can be calculated using the following equation:

$$D = \frac{1}{2}C_D\rho A|v|v, \tag{7}$$

where A is the frontal area of the dispersal unit and equal to πR^2. Then, we obtain a system of first-order ODEs:

$$\begin{cases} \dot{x} = v_x \\ \dot{v}_x = -D_x \\ \dot{y} = v_y \\ \dot{v}_y = -g - D_y, \end{cases} \tag{8}$$

where the gravitational acceleration, g, is equal to 9.81 m/s². We have solved the system of the differential equations by using Runge-Kutta fifth-order accurate (RK45) solver in the Python package SciPy. The dispersal distance of a dispersal unit was defined as the landing position on the x-axis with reference to the origin, i.e. the position of the style.

3. Results

3.1. Functional segments of floret

Florets of *H. radicata* can be subdivided into three functional segments from top to bottom: an exposed distal style, an anther tube in the middle, and five basal filaments (Figs. 1, 3b).

201 Mechanical testing of the florets revealed distinct stiffness of the three segments. The style,

202 which passes through the anther tube and is exposed at its distal segment, has the lowest

203 spring constant (N = 9, $K = 0.2 \pm 0.1$ Nm^{-1}) among other segments. It is embraced by the

204 stiff anther tube, which features the highest spring constant (N = 10, $K = 6.5 \pm 2.7$ Nm^{-1}).

205 The anther tube is connected to the petal at its proximal part by five filaments, which

206 altogether have an intermediate spring constant (N = 15, $K = 2.3 \pm 1.9$ Nm^{-1}). The spring

207 constants of the three segments are significantly different from each other (Tukey multiple

208 comparisons of means, filaments vs style: p-value $= 0.01$; anther tube vs style: p-value $=$

209 2.0×10^{-7}; anther tube vs filaments: p-value $= 1.3 \times 10^{-4}$).

211 3.2. Mechanics of pollen dispersal

213 The high-speed video analysis enabled us to investigate stylar oscillations. Fig. 2i-k shows

214 three snapshots of the stylar oscillation from release to return. When the floret was

215 deflected, the elastic energy was mainly stored in the proximal part of the flexible style and

216 the filaments. However, no obvious deformation was observed in the anther tube (Fig. 2i).

217 Upon the release, the style snapped back in the opposite direction of the applied

218 displacement, initiating the first half cycle of oscillation. The oscillation decayed quickly,

219 and the style returned to the resting position (N = 55, damping ratio $\zeta = 0.182 \pm 0.05$,

220 frequency $f = 119 \pm 23$ Hz) (Fig. 5b).

221 Based on the high-speed videos, we found that the first half cycle caused the major

222 pollen dispersal (Fig. 2k). The maximum acceleration in each half cycle decreased over time

223 (Fig. 5b and 5c, left), so that they were significantly different from each other (Tukey

224 multiple comparisons of means, large deflections, a_1 vs a_2: p-value < 0.001, a_2 vs a_3: p-value

225 $= 0.0013$, a_3 vs a_1: p-value < 0.001; small deflections, a_1 vs a_2: p-value $< 2.2 \times 10^{-6}$, a_2 vs a_3:

226 p-value $= 0.0098$, a_3 vs a_1: p-value < 0.001).

227 As shown in Fig. 5c, for both large and small deflections, the maximum stylar

228 acceleration in the first half cycle, a_1, exceeded the critical acceleration, a_c. However, the

229 maximum acceleration in the subsequent half cycles (i.e. a_2 and a_3, respectively) largely

230 overlapped with the critical acceleration, and the third peak, a_3, mostly became lower than

231 the median critical acceleration.

232 The velocity corresponding to the maximum acceleration in the first half cycle, v_1,

233 was by far the highest and significantly different from velocities corresponding to the

234 accelerations in the second and third peaks, v_2 and v_3 (Fig. 5c, right) (Tukey multiple

comparisons of means, large deflections, v_1 vs v_2: p-value < 0.001, v_2 vs v_3: p-value = 0.97, v_3 vs v_1: p-value < 0.001; small deflections, v_1 vs v_2: p-value < 0.001, v_2 vs v_3: p-value = 0.77, v_3 vs v_1: p-value < 0.001).

We examined the relationship between the number of dispersed grains, n_d, with 3 potentially influential parameters of frequency, damping ratio, and maximum acceleration of the styles (Fig. 5a). While no correlation was found between the frequency or damping ratio with the number of dispersed grains (Pearson's product-moment correlation, f vs n_d: t = -0.22 df = 22, p-value = 0.82; ζ vs n_d: t = -0.74, df = 22, p-value = 0.47), we found a significant correlation between maximum acceleration and the number of dispersed grains (Pearson's product-moment correlation, max a vs n_d: t = 3.2, df = 22, p-value = 0.004). The relatively low coefficient of determination (R^2 = 0.32) can be attributed to variations in the amount of pollen grains on the examined styles.

3.3. Effects of deflection magnitude on pollen dispersal

Large deflections resulted in significantly higher accelerations in the first two peaks, but not in the subsequent peaks (t-test, a_1: t = 3.90, df = 52, p-value = 0.00028; a_2: t = 2.03, df = 52, p-value = 0.047; a_3: t = 0.96, df = 52, p-value = 0.34) (Fig. 5c, left). They also lead to a significantly higher number of dispersed grains, in comparison with small deflections (t-test, t = -2.34, df = 16, p-value = 0.034). This is reflected by the positive correlation between the maximum acceleration in the first half cycle, a_1, and the number of dispersed grains, n_d, demonstrated in Fig. 5a. Whereas large deflection caused higher corresponding velocity at only the first acceleration peak (t-test, v_1: t = 6.10, df = 52, p-value < 0.001; v_2: t = 1.13, df = 52, p-value = 0.26; v_3: t = 1.66, df = 52, p-value = 0.10) (Fig. 5c, right).

In contrast, as shown in Fig. 6a, the different deflection magnitudes had no significant effect on pollen distribution (t-test, t = -0.96, df = 397, p-value = 0.34). The stylar oscillation tended to catapult the dispersal units against the deflection direction with a median dispersal distance of 5.5 mm, in both large and small deflections. Surprisingly, 93.5% of the dispersal units landed within 15.8 mm from the origin, which is equal to the mean radius of flowerheads of *H. radicata*.

Although our simulations showed a broader peak of the dispersal distances (Fig. 6), the simulated pollen distribution exhibited similar trends as the measurements: the tendency of pollen dispersal toward a pollinator and the restrained dispersal distances within the size of the flowerhead.

269   Fig. 7a shows the representative simulated trajectories of dispersal units based on the

270   tracked stylar oscillations (red asterisks), initiated by the small and large deflections of the

271   styles. Fig. 7b shows estimated detachment points, where eq.3 was satisfied. Large

272   deflections widened the range of detachment points, in comparison to small deflections.

273   They also shifted the detachment points towards lower values in both the x and y axes,

274   compared with the small deflections (Kruskal test, x-axis: chi-squared = 29.9, p-value <

275   0.001; y-axis: chi-squared = 45.2, p-value < 0.001). It means that the larger deflections caused

276   pollen detachment closer to the ground and further from a pollinator than the smaller

277   deflections.

278

279

280   4.   Discussion

281

282   This study is focused on the oscillation of the style triggered by an initial deflection and its

283   potential as a ballistic lever that catapults pollen towards a flower-visiting pollinator. Since

284   the pollen catapult is a passive spring-driven system, the adaption to a variety of deflection

285   magnitudes is likely to be a key to the successful delivery of pollen to a pollinator and

286   minimizing the waste of dispersed pollen. Here we will discuss the potential role of

287   morphological and mechanical features of the reproductive part of a floret as well as the

288   adhesive properties of pollen in the pollen catapult system.

289

290   4.1. Floret: a functional composite

291

292   Similar to other species in the Asteraceae family[32], florets of *H. radicata* can be regarded as

293   composites made from three morphologically distinctive segments (Figs. 1, 3b). It is known

294   that each of the segments plays an essential role in pollen presentation [18,19,33]. Do they also

295   contribute to the pollen catapulting towards visiting pollinators, after pollen presentation?

296   To present pollen and successfully deliver it to visiting pollinators, the floret with the

297   pollen-bearing style should meet these requirements: (1) high mechanical compliance

298   during contact to store elastic energy and prevent damage and (2) catapult pollen towards a

299   pollinator by adapting to varying magnitudes of initial deflections.

300   At the distal end of a floret, the flexibility of the pollen-bearing style enables high

301   compliance under contact as well as energy storage for pollen catapult after release (Fig. 2i-

302   k). The middle segment of the floret is reinforced by the anther tube, which functions as a

303   support for the slender style during contact and stabilizes the shape of the floret during

304   non-contact periods. Previous studies have shown that the deformation of a flexible

305   cantilever with a high aspect ratio occurs proximally to the deflection points[34]. Therefore, in

306   the case of physical contact at the style, the elastic energy would be stored in the broad

307   proximal area of the floret. However, the reinforcement of the proximal segment of the

308   floret by the anther tube prevents the deformation of this segment, limiting the amount of

309   energy stored and released at the distal end of the style. This is likely to restrict excessive

310   stylar acceleration, and thus reduce the number of catapulted pollen grains.

311   The other energy-storing segment, consisting of filaments, is located at the base of the

312   floret. This segment, with its intermediate stiffness, functions as a flexible joint. It enhances

313   the mechanical compliance of the whole structure in contact, and therefore, enables

314   adaptation to the different deflection magnitudes. When the large initial deflection is

315   applied, the flexible joint helps to recline the whole floret (Figs. 2i, 7a). As mentioned earlier,

316   larger deflections lower the detachment points and shift them further from a pollinator (Fig.

317   7b). This is likely to counterbalance the increased initial velocity of catapulted dispersal

318   units (Fig. 5c, v_i) to still distribute pollen within the same range of distances, independent of

319   the initial deflection magnitudes (Fig. 6a).

320

321

322

323   ## 4.2. Pollen adhesion

324

325   Some animals, such as insects and elks, clean themselves by vibrating their hairs to remove

326   accumulated particles[35,36]. In such systems, the natural frequency governs particle

327   detachment:

328      $$a = Sf^2,\qquad\qquad\qquad\qquad(12)$$

329   where a is the acceleration, S is the spacing between the hairs, which dictates the maximum

330   deflection of the hairs, and f is the natural frequency[35]. However, here, we did not find

331   correlations between the natural frequency and the number of dispersed grains (Fig. 5a) or

332   between the natural frequency and maximum linear acceleration (Fig. S1).

333   It is important to mention that the major pollen detachment occurs only in the first

334   half oscillation cycle. Hence, the general oscillatory frequency has very little influence on

335   pollen detachment. To restrict the pollen detachment only to the first half cycle, the critical

acceleration, a_c, should be less than the first maximum acceleration, a_1, but greater than maximum accelerations in any other oscillation cycles (Fig. 5c, left).

As shown in eq.3, the critical acceleration depends not only on the pollen-style adhesion, but also on the pollen-pollen adhesion, which governs the number of pollen grains in a dispersal unit. The weaker pollen-pollen adhesion, therefore, decreases the number of grains in a dispersal unit, in comparison to $n = 13$ measured here. Since the inertial force is proportional to the mass of the dispersal unit, a smaller number of pollen in a dispersal unit can challenge its detachment from the style. If the number of grains is as small as $n = 3$, the median critical acceleration would be greater than most of the measured maximum stylar accelerations, and this would completely emasculate the pollen catapult. In contrast, higher pollen-pollen adhesion would result in a higher number of grains in the dispersal units. This would, on the other hand, lead to a prolonged, and probably, isotropic pollen dispersal (both towards and against the pollinator) and, therefore, increase the number of wasted pollen. Hence, for a guided pollen dispersal towards a pollinator, pollen adhesion and the size of dispersal units should be kept in a certain range.

Unlike wind-pollinated species, the insect-pollinated ones are covered by a thick layer of a viscous oily substance called pollenkitt[37], which helps to form large dispersal units by bonding pollen grains together[37,38]. In addition to its general function as "pollen adhesive", we recently showed that pollenkitt inhibits pollen adhesion by weakening water capillary attraction[25]. Therefore, we can assume that pollenkitt may play a role in maintaining pollen adhesion in a specific range. Future studies are needed to quantitatively investigate the role of pollenkitt in pollen-pollen adhesion.

4.3. Phase shift in the first half oscillation cycle

Once the pollen detachment occurs, the pollen dispersal is mainly governed by the initial velocity of the dispersal units, rather than their acceleration. Hence, the velocity corresponding to each maximum stylar acceleration (Fig. 5c, right) is another key for the guided pollen dispersal towards a pollinator.

Unlike the stylar acceleration peaks, the corresponding stylar velocities abruptly decayed, so that the velocities corresponding to the second and third maximum accelerations (i.e., v_2 and v_3, respectively) were not significantly different from each other (Fig. 5c, right). Only the first corresponding velocity, v_1, is significantly higher than the

369 others, because of the phase shift between the stylar acceleration and velocity at the first half
370 cycle.

371 In a free oscillation, the displacement, $x(t)$, is given as:

372 $$x(t) = A\cos(\omega t - \phi), \tag{13}$$

373 where A is an arbitrary constant and ω is the angular frequency. Differentiating eq.13 with
374 respect to t gives the velocity $v(t)$ as:

375 $$v(t) = \omega A\cos\left(\omega t - \phi + \frac{\pi}{2}\right), \tag{14}$$

376 In the same manner, the acceleration, $a(t)$, is given as:

377 $$a(t) = \omega^2 A\cos(\omega t - \phi + \pi), \tag{15}$$

378 The phase difference between the acceleration and velocity is equal to $\frac{\pi}{2}$, or a quarter of an
379 oscillation cycle. Therefore, in the free oscillation, the corresponding velocities at the
380 moment of acceleration peaks, ideally, are the local minima. As shown in Fig. 5b, this typical
381 phase difference appeared in the stylar oscillations, resulting in the extremely small values
382 of v_2 and v_3. However, the first corresponding velocity, v_1, was shifted from the local
383 minimum; therefore, v_1 was by far the highest than other corresponding velocities. The
384 cause of the phase shift is seemingly due to the style sliding over the insect pin during the
385 release, and therefore, a detailed study on this topic will be required in the future.

386
387
388 ## 4.4. Biological significance

389

390 Asteraceae are known for attracting various insect pollinators[20]. Their robust adaptability
391 makes a number of them notorious invasive species[39,40]. To enable their versatile
392 reproduction, Asteraceae may use multiple strategies to secure pollen transfer to diverse
393 pollinators. Each pollinator species may have its own difficulties to be a functional pollen
394 vector for the benefit of plants. Bees, for example, are both pollen-transporting vectors and
395 pollen consumers. Actively collected pollen grains, are soaked with their saliva and are
396 packed in a specialized pollen-carrying apparatus, and no longer available for
397 pollination[21,41]. Some pollinators, such as flies from the family Bombyliidae, with their
398 specialized long mouthparts and slender limbs less frequently make physical contact with
399 styles on flowers, yet are able to obtain nectary rewards[42] (Fig. 2f-h).

400 In this paper, we discussed that the superficially unremarkable floret of *H. radicata*,
401 by optimizing its (1) morphological and mechanical properties, (2) adhesive properties of
402 pollen, and (3) phase difference between the stylar acceleration and velocity, functions as a

projectile tool to catapult pollen towards pollinators. The airborne pollen dispersal system is advantageous to deliver pollen to various body parts of pollinators, including their safe sites, as well as to engage the long-limbed insects beyond the physical reach of the styles[43,44]. The attached pollen on the pollinators is potentially transferred to the stigma of other flowers by electrostatic attractions[45–48] or grooming[36]. It is also remarkable that more than 90% of the dispersal units landed within a region of the same size as that of the flowerhead. Therefore, even if the dispersal units fail to reach the target pollinator, they remain within the flowerhead, waiting for being transferred to the forthcoming pollinators.

It is well known that florets of Asteraceae consecutively mature from the outer row towards the central row. For many species of this family, including *H. radicata*, this means that young and most pollen-bearing styles are situated in the center of the flowerhead[49]. The tuned travel distance of the dispersal units, therefore, may explain the order of the floret maturity in Asteraceae. The working principles of the pollen catapult in Asteraceae are rooted in a common floral feature of the family. If this mechanism is found to be present in other species within the family, it could potentially contribute to the reproductive success of one of the largest families of flowering plants. However, future research is necessary to determine the prevalence of similar pollen dispersal mechanics in other species within the family

5. Conclusions

In this study, we suggested a novel pollen dispersal strategy resulting from the stylar oscillation of *H. radicata*. Based on the combination of high-speed motion analysis, mechanical tests, and numerical simulations, we found that the morphologically and mechanically distinctive segments composing the floret, as well as the optimal pollen adhesion, potentially contribute to (1) catapulting pollen towards a visiting pollinator while (2) minimizing the wasteful pollen dispersal by (3) adapting to a different amount of oscillation-inducing external deflections. Since the ballistic pollen dispersal arises from a standard floral morphology of Asteraceae, it can potentially play a role in the pollination of the most ubiquitous flowering family on the planet.

6. Acknowledgments

7. Funding

8. Data availability

The codes used in this study is available at https://www.notion.so/biomimetica/pollen-catapult-c75f8abd93e44ab7b03f6226b47d4446 .

9. Author contributions

S.I., H.R., and S.N.G. conceptualized the study. S.I. and H.R. designed the experiments. S.I. conducted the research, collected and analyzed the data. S.I. and H.R. participated in the data presentation. S.N.G. provided equipment and supervised the study. S.I. wrote the first draft. H.R. and S.N.G. edited the manuscript. All authors discussed the results and gave the final approval for publication.

10. Competing interests

The authors declare no competing or financial interests.
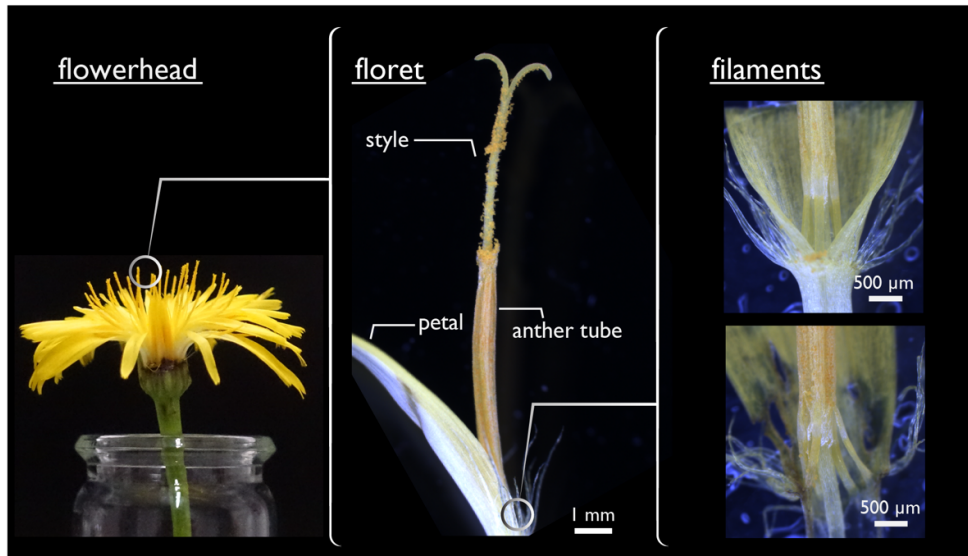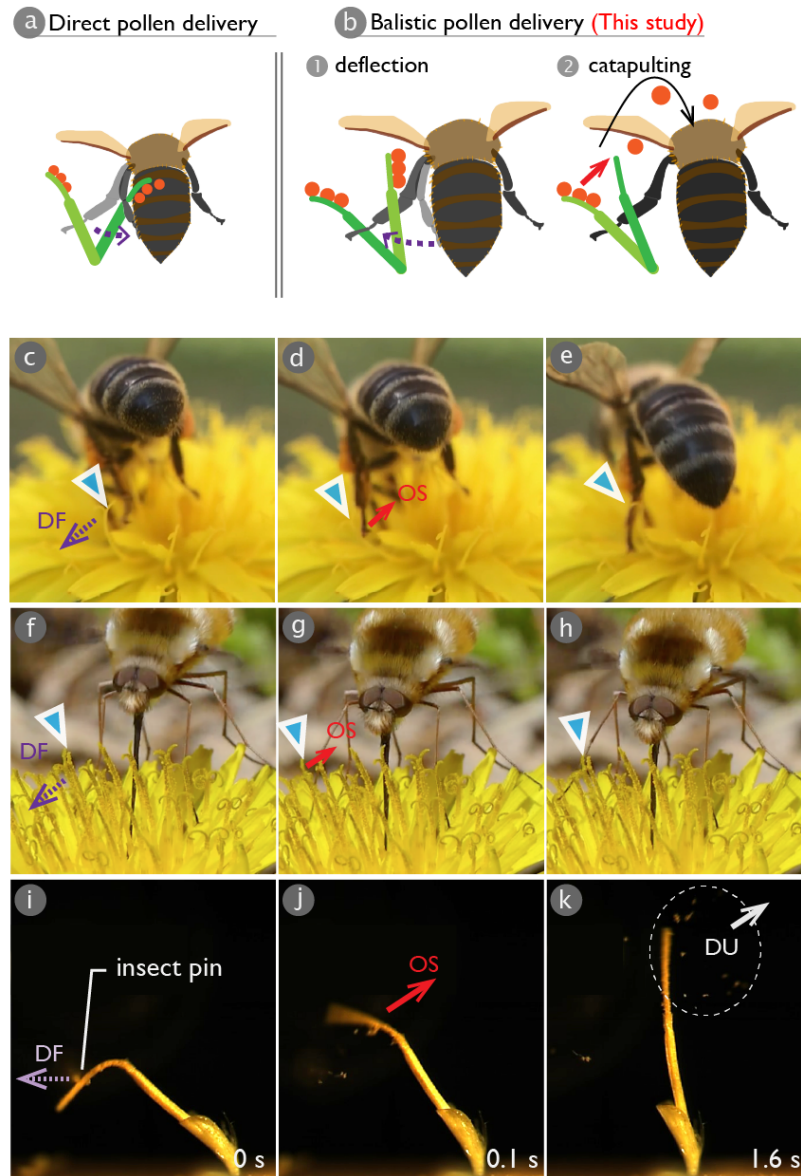
467

468

469 Figures

470

471

472

Fig. 1 Floral structures of *Hypochaeris radicata* at three different scales: a whole flowerhead (left) composed of many florets (middle), of which basal segment, so-called filaments, are magnified (right).

476

477

Fig. 2 (a,b) Conceptualization of the current study. A stylar deflection toward a pollinator causes a direct pollen delivery to the pollinator (a), whereas a deflection to the opposite direction enables a ballistic pollen delivery to the pollinator (b). (c-h) Interaction between insects and styles. A style, which positions are shown with blue triangles, was deflected by a limb of a bee *Apis mellifera* (c-e) or that of a fly from the family Bombyliidae (f-h). Upon the release, the style snaps back towards the insect. (d-f) Snapshots from a high-speed video of an oscillating style showing pollen dispersal after a larger deflection. DF: deflection, OS: oscillation, DU: pollen dispersal units.

488
489
490
491
492
493
494
495
496
497
498
499
500
501
502
503
504
505
506
507
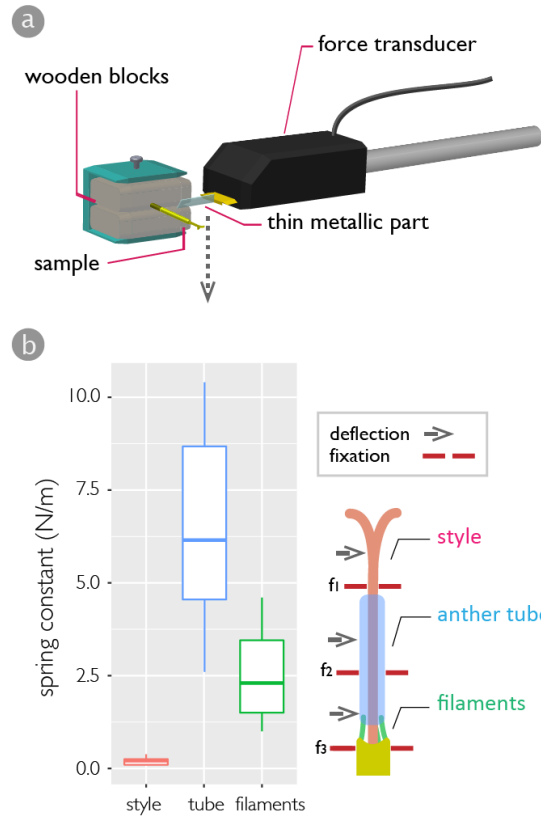508
509
510
511
512
513

514 Fig. 3 Mechanical characterization of florets. (a) The experimental setup. (b) Bar plots of the spring
515 constant of three different segments of florets. The illustration on the right-hand shows the fixations
516 and the locations of the applied deflection. specimens were fixed at f_1, f_2, and f_3 to measure the spring
517 constants of the style, anther tube, and filaments, respectively.

518

519
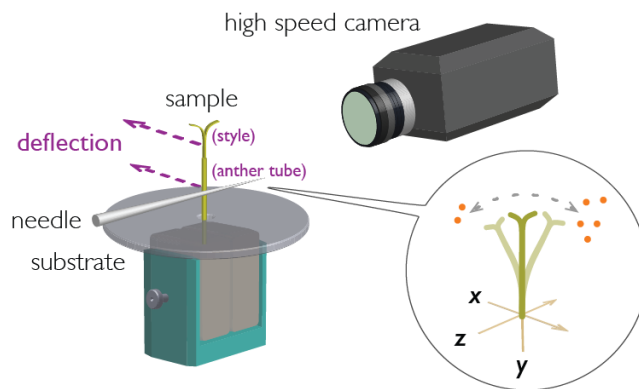
520 Fig. 4 The experimental setup of the oscillation experiments. The initial deflections, which triggered

521 the stylar oscillation, were applied to two different positions to cause two distinct deflection

522 magnitudes. The stylar oscillations were recorded by using a high-speed camera. The dispersed

523 pollen grains, catapulted by the stylar oscillations and landed on the circular substrates, were
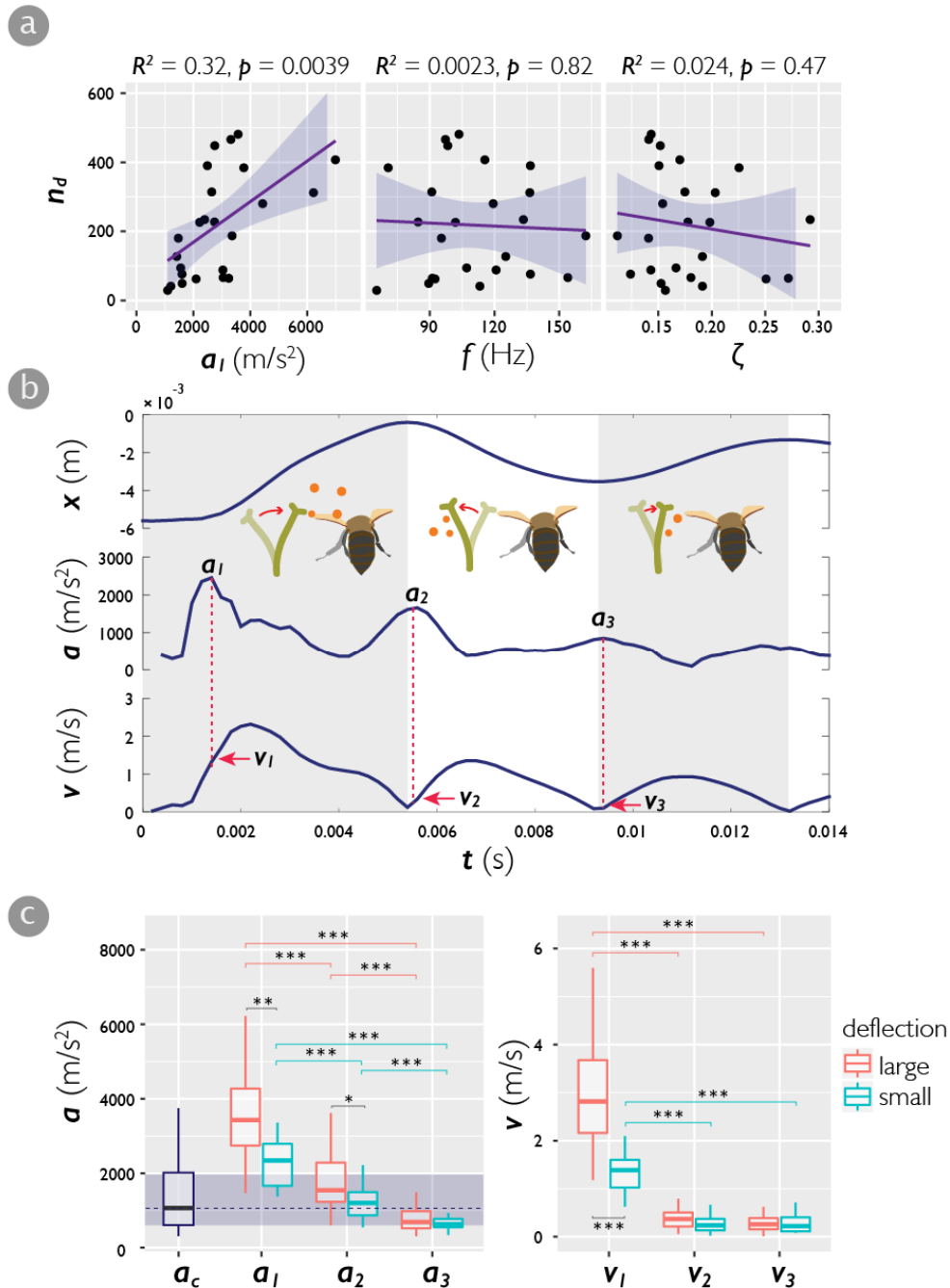
524 photographed from above.

525 Fig. 5 (a) Correlation analysis between the number of dispersed grains and each variable extracted

526 from the motion data: a_l (left), frequency f (middle), and damping ratio ζ (right). (b) Time series of the

stylar displacement *x*, linear acceleration *a*, and velocity *v*. The first, the second, and the third peak of

linear acceleration were denoted as a_1, a_2, and a_3, respectively. The corresponding velocities at the

moment of each acceleration peak were denoted as v_1, v_2, and v_3, respectively. The shadowed half

cycles show the regimes where pollen should be catapulted towards a pollinator if the pollen

detachment from the style occurs. (c) Bar plots of the acceleration peaks in stylar oscillations after

small or large deflections (left) and the corresponding velocities at each acceleration peaks (right). The

shadowed region with a vertical dashed line in the left-hand side figure shows the first and the third
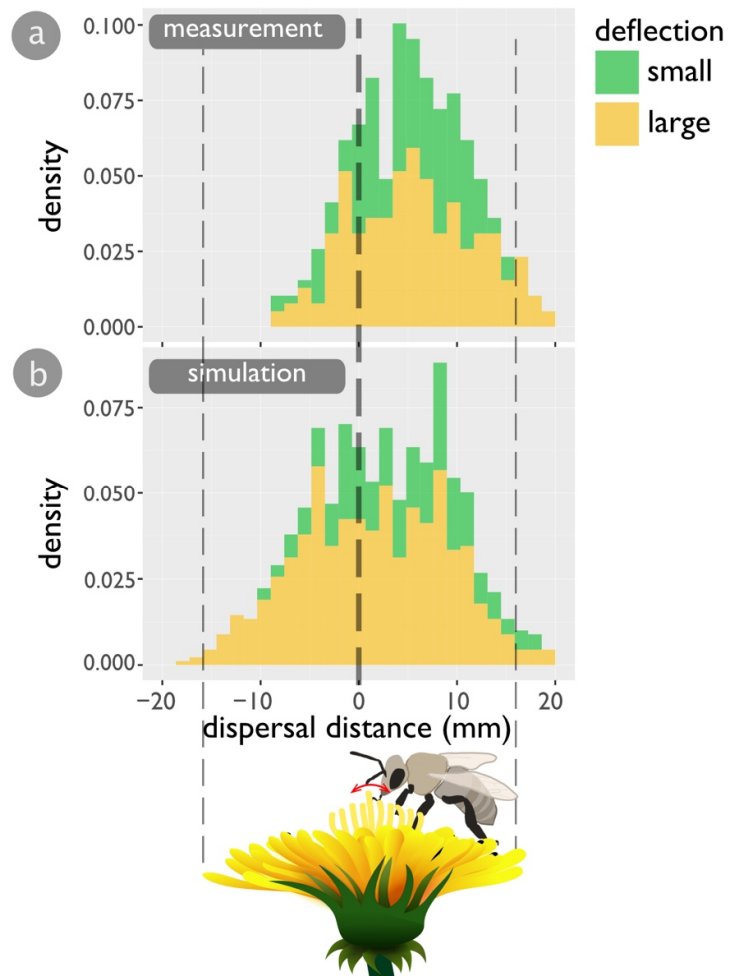
quantile, and the median value of the critical acceleration, a*c*. The critical acceleration is the required

acceleration to detach dispersal units from the style, calculated based on the measured pollen

adhesion on the style and the average number of pollen grains in a dispersal unit (n = 13).

Fig. 6 Stacked histograms of the distributions of dispersal units catapulted by stylar oscillations due

to small and large deflections: (a) measurement (N = 55) and (b) simulation.

541

542

543
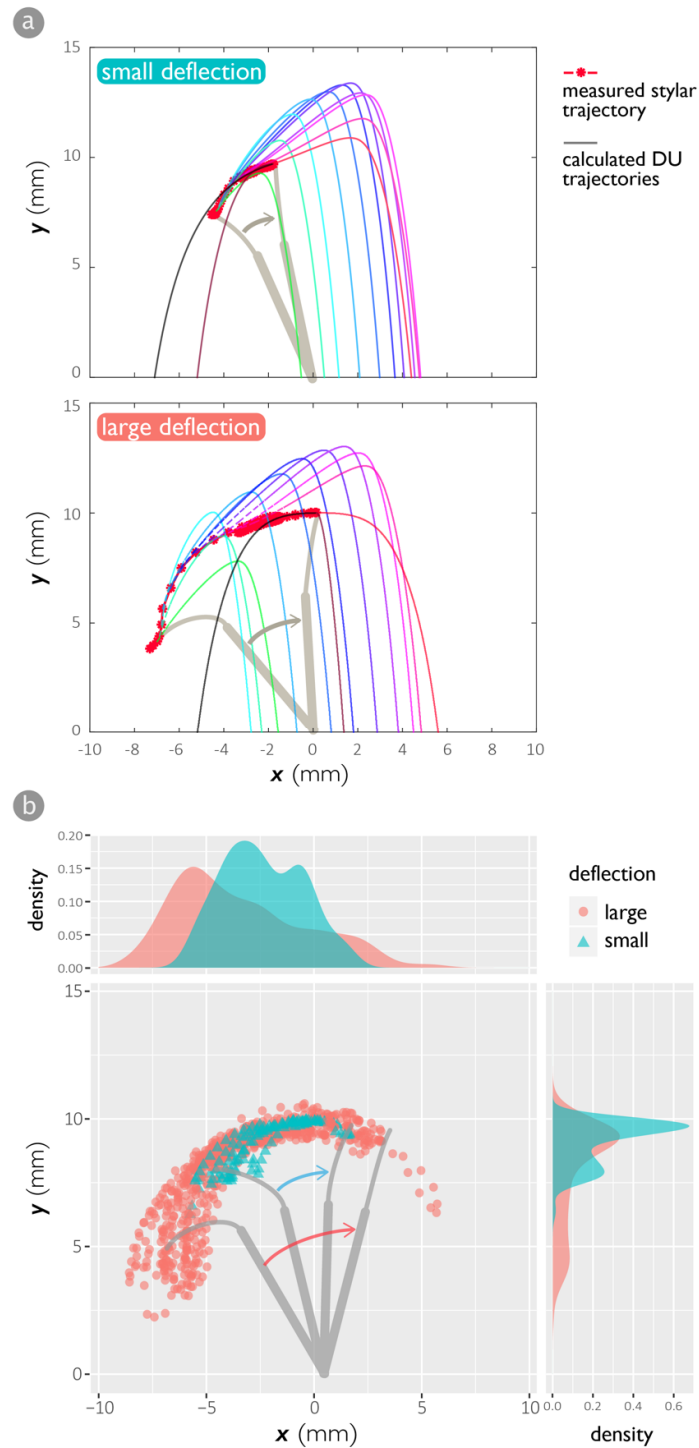
Fig. 7 (a) Calculated trajectories of dispersal units (thin solid lines with varying colors) based on the

measured trajectories of stylar oscillations (red asterisks) initiated by different deflection magnitudes.

546   Different trajectories of the dispersal units were colored differently to make them distinguishable. (b)

547   Estimated detachment points of stylar oscillations initiated by different deflection magnitudes.

548

549

550

551

552   11. References

553

554   1.   van der Kooi, C. J., Vallejo-Marín, M. & Leonhardt, S. D. Mutualisms and (A)symmetry in

555   Plant–Pollinator Interactions. *Curr. Biol.* **31**, R91–R99 (2021).

556   2.   Westerkamp, C. Pollen in Bee-Flower Relations. *Bot. Acta* **109**, 325–332 (1996).

557   3.   Gurung, V., Yuan, Y. W. & Diggle, P. K. Comparative analysis of corolla tube development

558   across three closely related Mimulus species with different pollination syndromes. *Evol. Dev.*

559   **23**, 244–255 (2021).

560   4.   Katzer, A. M., Wessinger, C. A. & Hileman, L. C. Nectary size is a pollination syndrome trait

561   in Penstemon. *New Phytol.* **223**, 377–384 (2019).

562   5.   Claßen-Bockhoff, R. *et al.* The staminal lever mechanism in Salvia L. (Lamiaceae): A key

563   innovation for adaptive radiation? *Org. Divers. Evol.* **4**, 189–205 (2004).

564   6.   Bröderbauer, D., Weber, A. & Diaz, A. The design of trapping devices in pollination traps of

565   the genus Arum (Araceae) is related to insect type. *Bot. J. Linn. Soc.* **172**, 385–397 (2013).

566   7.   Vereecken, N. J. *et al.* Pre-adaptations and the evolution of pollination by sexual deception:

567   Cope's rule of specialization revisited. *Proc. R. Soc. B Biol. Sci.* **279**, 4786–4794 (2012).

568   8.   Edwards, J., Whitaker, D., Klionsky, S. & Laskowski, M. A record-breaking pollen catapult.

569   *Nature* **435**, 2005 (2005).

570   9.   Switzer, C. M., Combes, S. A. & Hopkins, R. Dispensing Pollen via Catapult: Explosive Pollen

571   Release in Mountain Laurel (Kalmia latifolia). *Am. Nat.* **191**, 767–776 (2018).

572   10.   Taylor, P. E., Card, G., House, J., Dickinson, M. H. & Flagan, R. C. High-speed pollen release in

573   the white mulberry tree, Morus alba L. *Sex. Plant Reprod.* **19**, 19–24 (2006).

574   11.   Michener, C. D. An interesting method of pollen collecting by bees from flowers with tubular

575   anthers. *Biol. Trop* **10**, 167–175 (1962).

576   12.   King, M. J., Buchmann, S. L. & Spangler, H. Activity of asynchronous flight muscle from two

577   bee families during sonication (buzzing). *J. Exp. Biol.* **199**, 2317–2321 (1996).

578   13.   Marcus J King & Buchmann, S. L. Bumble Bee-Initiated Vibration Release Mechanism of

579   Rhododendron Pollen. *America (NY).* **82**, 1407–1411 (2011).

580   14.   Vallejo-Marín, M. Buzz pollination: studying bee vibrations on flowers. *New Phytol.* **224**, 1068–

581   1074 (2019).

582   15.   Vallejo-Marín, M., Pereira Nunes, C. E. & Russell, A. L. Anther cones increase pollen release in

583   buzz-pollinated Solanum flowers. *Evolution (N. Y)*. **76**, 931–945 (2022).

584   16.   Jankauski, M., Ferguson, R., Russell, A. & Buchmann, S. Structural dynamics of real and

585   modelled Solanum stamens: Implications for pollen ejection by buzzing bees. *J. R. Soc. Interface*

586   **19**, (2022).

587   17.   Barreda, V. D. *et al.* Early evolution of the angiosperm clade Asteraceae in the Cretaceous of

588   Antarctica. *Proc. Natl. Acad. Sci. U. S. A.* **112**, 10989–10994 (2015).

589   18.   Erbar, C. & Leins, P. Diversity of styles and mechanisms of secondary pollen presentation in

590   basal Asteraceae-New insights in phylogeny and function. *Flora* **217**, 109–130 (2015).

591   19.   Leins, P. & Erbar, C. Secondary pollen presentation syndromes of the Asterales — a

592   phylogenetic perspective. *Bot. Jahrbücher* **127**, 83–103 (2006).

593   20.   Alarcón, R., Waser, N. M. & Ollerton, J. Year-to-year variation in the topology of a plant-

594   pollinator interaction network. *Oikos* **117**, 1796–1807 (2008).

595   21.   Parker, A. J. *et al.* Pollen packing affects the function of pollen on corbiculate bees but not non-

596   corbiculate bees. *Arthropod. Plant. Interact.* **9**, 197–203 (2015).

597   22.   Matherne, M. *et al.* Biomechanics of pollen pellet removal by the honey bee. *J. R. Soc. Interface*

598   **18**, (2021).

599   23.   Roberts, R. B. & Vallespir, S. R. Specialization of Hairs Bearing Pollen and Oil on the Legs of

600   Bees (Apoidea: Hymenoptera)1. *Ann. Entomol. Soc. Am.* **71**, 619–627 (2015).

601   24.   Snodgrass, R. . The anatomy of the honey bee. *Cornell Univ. Press* (1910).

602   25.   Ito, S. & Gorb, S. N. Fresh 'pollen adhesive' weakens humidity-dependent pollen adhesion.

603   *ACS Appl. Mater. Interfaces* **11**, 24691–24698 (2019).

604   26.   Ito, S. & Gorb, S. N. Attachment-based mechanisms underlying capture and release of pollen

605   grains. *J. R. Soc. Interface* **16**, 20190269 (2019).

606   27.   Doi, M., Ito, M. & Auld, B. A. Growth and reproduction of Hypochoeris radicata L. *Weed Biol.*

607   *Manag.* **6**, 18–24 (2006).

608   28.   Picó, F. X., Ouborg, N. J. & Van Groenendael, J. Influence of selfing and maternal effects on

609   life-cycle traits and dispersal ability in the herb Hypochaeris radicata (Asteraceae). *Bot. J. Linn.*

610   *Soc.* **146**, 163–170 (2004).

611   29.   Brown, D. & Cox, A. J. Innovative Uses of Video Analysis. *Phys. Teach.* **47**, 145–150 (2009).

612   30.   Huang, W. & Yu, L. Serial symmetrical relocation algorithm for the equal sphere packing

613   problem. *Appl. Res. Comput.* 25 (2012).

614   31.   Jones, A. M. & Knudsen, J. G. Drag coefficients at low Reynolds numbers for flow past

615   immersed bodies. *AIChE J.* **7**, 20–25 (1961).

616   32.   Meiri, L. & Dulberger, R. Stamen filament structure in the Asteraceae: the anther collar. *New*

617   *Phytol.* **104**, 693–701 (1986).

618   33.   Erbar, C. & Leins, P. Portioned pollen release and the syndromes of secondary pollen

619   presentation in the Campanulales-Asterales-complex. *Flora* **190**, 323–338 (1995).

620   34.   Rajabi, H. *et al.* Both stiff and compliant: Morphological and biomechanical adaptations of

621   stick insect antennae for tactile exploration. *J. R. Soc. Interface* **15**, 20180246 (2018).

622   35.   Amador, G. J. & Hu, D. L. Cleanliness is next to godliness: Mechanisms for staying clean. *J.*

623   *Exp. Biol.* **218**, 3164–3174 (2015).

624   36.   Amador, G. J. *et al.* Honey bee hairs and pollenkitt are essential for pollen capture and

625   removal. *Bioinspiration and Biomimetics* **12**, 026015 (2017).

626   37.   Pacini, E. & Hesse, M. Pollenkitt - Its composition, forms and functions. *Flora* **200**, 399–415

627   (2005).

628   38.   Lisci, M., Cardinali, G. & Pacini, E. Pollen dispersal and role of pollenkitt in Mercurialis annua

629   L. (Euphorbiaceae). *Flora* **191**, 385–391 (1996).

630   39.   Thebaud, C. & Abbott, R. J. Characterization of invasive Conyza species (Asteraceae) in

631   Europe: Quantitative trait and isozyme analysis. *Am. J. Bot.* **82**, 360–368 (1995).

632   40.   Hao, J. H., Qiang, S., Chrobock, T., van Kleunen, M. & Liu, Q. Q. A test of baker's law:

633   Breeding systems of invasive species of Asteraceae in China. *Biol. Invasions* **13**, 571–580 (2011).

634   41.   Thorp, A. R. W. The collection of pollen by bees. *Plant Syst. Evol.* **222**, 211–223 (2000).

635   42.   Kastinger, C. & Weber, A. Bee-flies (Bombylius spp., Bombyliidae, Diptera) and the pollination

636   of flowers. *Flora* **196**, 3–25 (2001).

637   43.   Macior, L. W. An experimental study of the floral ecology of Dodecatheon meadia. *Am. J. Bot.*

638   **51**, 96–108 (1964).

639   44.   Koch, L., Lunau, K. & Wester, P. To be on the safe site – Ungroomed spots on the bee's body

640   and their importance for pollination. *PLoS One* **12**, 1–16 (2017).

641   45.   Vaknin, Y., Gan-mor, S., Bechar, A., Ronen, B. & Eisikowitch, D. Are flowers morphologically

642   adapted to take advantage of electrostatic forces in pollination? *New Phytol.* **152**, 301–306

643   (2001).

644   46.   Eisikowitch, D., Vaknin, Y., Bechar, A., Ronen, B. & Gan-Mor, S. The role of electrostatic forces

645   in pollination. *Plant Syst. Evol.* **222**, 133–142 (2005).

646   47.   Bowker, G. E. & Crenshaw, H. C. Electrostatic forces in wind-pollination-Part 1: Measurement

647   of the electrostatic charge on pollen. *Atmos. Environ.* **41**, 1587–1595 (2007).

648   48.   Bowker, G. E. & Crenshaw, H. C. Electrostatic forces in wind-pollination-Part 2: Simulations of

649   pollen capture. *Atmos. Environ.* **41**, 1596–1603 (2007).

650   49.   Elizabeth M. Harris. Inflorescence and floral ontogeny in asteraceae: A synthesis of historical

651   and current concepts. *Bot. Rev.* **61:93**, (1995).

652